JOURNAL OF MECHANICAL ENGINEERING, SCIENCE, AND INNOVATION
ITATS
Research Article

Comparative Structural Performance Evaluation of Modified Stopper Mounting Designs in Conveyor Systems Using Finite Element Simulation

Journal of Mechanical Engineering, Science, and Innovation
e-ISSN: 2776-3536
2026, Vol. 6, No. 1
DOI: 10.31284/j.jmesi.2026.v6i1.8501
ejurnal.itats.ac.id/jmesi

Maulidia Hendriani[1], Andoko Andoko[1*], Riduwan Prasetya[1], and Yahya Zakaria[1]

[1]Department of Mechanical and Industrial Engineering, Faculty of Engineering, State University of Malang, Jl Semarang 5, Malang City, Indonesia

Corresponding author:
Andoko andoko
State University of Malang, Indonesia
Email: andoko.ft@um.ac.id

Abstract

This study investigates the structural performance of three stopper mounting designs for conveyor systems using finite element simulations in ANSYS Workbench. The analysis was conducted using a static structural method, where a vertical downward load of 103.43 N converted from the total weight of the stopper was applied to the structure, and fixed support boundary conditions were assigned at the mounting base. We compared the original design with two modified versions, including one reinforced with stiffening ribs. We evaluated each model under static loads by measuring total deformation, equivalent stress, elastic strain, and safety factor. Compared to the original design, MD 1 reduced total deformation by 88.42%, elastic strain by 53.04%, and equivalent stress by 30.72%, while increasing the safety factor by 0.94%. These improvements were achieved without significantly increasing material usage. The addition of stiffening ribs effectively directed internal forces, stabilized stress zones, and enhanced structural resilience. The original design, while functional, exhibited high deformation and uneven stress distribution that limited its suitability for precision-dependent operations. Reinforcing the geometry proved essential in achieving better mechanical performance and durability. This validates the use of local structural enhancement as a key strategy in mechanical design. The findings contribute to automation system development by highlighting the importance of local reinforcement in precision-oriented automation components.

Keywords: *: Stopper mounting, finite elemet analysis, conveyor ssystem*

Received: December 19, 2026; Received in revised: March 19, 2026; Accepted: March 25, 2026
Handling Editor: Ayu Setyaning Poesoko and Michele Bici

INTRODUCTION

The manufacturing industry is undergoing accelerated technological transformation through the implementation of integrated automation and digitalization [1], [2].

Improvements in the efficiency, consistency, and flexibility of production processes are being driven by advances in intelligent control-based systems, robotics, and industrial information technology [3], [4]. Automation transforms production systems and accelerates product flow while reducing the manual workload [5], [6], [7]. Conveyor systems play a strategic role in facilitating the smooth movement of products. The reliability of these systems is greatly influenced by the quality of their structural components, including supporting units that are often considered minor [8].

One such component is the mounting stopper, which holds or positions the product accurately at specific points in the process. Despite its small size, the stopper's precise function determines the success of the overall system. In the current implementation, the stopper is mounted in a free-standing design that is not directly connected to the main conveyor structure. This design offers great flexibility because it can be moved as needed. However, this design also poses a serious risk to the stability of the position. The mounting stopper can shift from its calibration point if nudged by an operator or client. This shift directly impacts the precision of product placement and can lead to production flow disruptions, dimensional mismatches, and potential product rejections in the long run. The demands on the flexibility and precision of support components increase as product variations evolve and production system configurations change [9]. In modern manufacturing settings characterized by high-mix, low-volume output and frequent setup changes, such instability in structural support elements becomes a critical liability. A small misalignment in stopper position can cascade into significant production losses due to rework, recalibration delays, or out-of-spec parts. The old design has effectively performed its basic functions so far. Its structural performance remains relevant under stable and repetitive working conditions. However, the need for improved design efficiency and adaptability arises when the system faces more diverse workloads and continuously changing product conditions [10]. Therefore, more robust and efficient geometric designs are required without sacrificing flexibility. Innovations should focus on achieving more even load distribution and extending component life through local structural improvements, such as adding stiffening ribs or engineering fulcrums. Key aspects in creating a more robust system include cross-sectional shape, force distribution, and fulcrum position [11].

The lack of prior research on stopper mounting components presents an opportunity for engineering simulation-based analysis. Several previous studies have explored the structural behavior of conveyor system components using numerical methods. However, the focus of these studies has remained on large-scale, fixed frameworks rather than on modular subcomponents. Dong Zheng [12] developed a static strength analysis software using ANSYS and MATLAB to evaluate conveyor head tripod components under loading conditions. This study successfully demonstrated the use of simulation tools for predicting stress distribution and identifying critical areas prone to failure. However, the scope was restricted to rigid, symmetric tripod structures that are permanently fixed, rendering the findings inapplicable to mobile or freestanding elements. Furthermore, the study did not address localized strain responses or geometric modifications aimed at increasing stability under operator-induced disturbances. Gustavo Fruet and Letícia Fleck Fadel Miguel [13] proposed a comprehensive methodology for mass optimization in steel structural systems, specifically for supporting columns and galleries in bulk conveyor applications. Their contribution lies in minimizing structural weight while preserving mechanical integrity through advanced topology strategies. While this study advanced efficient design practices for static infrastructure, it lacked analysis of stress propagation in compact geometries where deformation control is critical. Furthermore, the investigation did not delve into the realm of reinforcement strategies, which include the incorporation of stiffening ribs. These strategies are frequently indispensable in averting flexural instability in components of reduced size

that lack external support. Meanwhile, Wheeler and Robinson [14] concentrated on implementing practical design improvements and reliability assessments in belt conveyor systems. This was achieved by identifying system-level weaknesses and proposing corrective actions. Their insights have the potential to yield valuable recommendations for enhancing durability and mechanical performance in complex transport systems. However, the study placed emphasis on macro-level operational issues without incorporating simulation-based structural analysis of subcomponents, such as mounting stoppers. Additionally, the study did not examine how minor misalignments or geometric deficiencies in local supports could affect overall process accuracy and repeatability. Collectively, these studies provide important frameworks for analyzing structural integrity in conveyor systems. However, none have examined the mechanical behavior of stopper mounting components under static loading. However, there is a paucity of research evaluating the effects of localized geometry modifications on stress dispersion, strain distribution, or deformation minimization. This research addresses that critical gap by applying finite element simulations to assess the performance of various stopper mounting designs, with particular focus on how geometric reinforcements influence their structural reliability in precision automation environments.

To address this gap, the present study applies a simulation-based design analysis using the finite element analysis (FEA). This approach allows for identification of critical stress zones, assessment of deformation behavior, and visualization of strain concentration patterns without relying on physical prototypes [15], [16], [17]. Exploring geometric variants further enables engineers to understand how design modifications influence structural performance [18], making the development process more informed, efficient, and cost-effective than conventional trial-and-error methods. The advantages of simulation serve as a foundation for creating robust and optimized mechanical designs for industrial automation [19]. This research aims to evaluate how different geometric configurations of stopper mounting affect structural performance under static loading. The study focuses on total deformation, von Mises stress distribution, equivalent elastic strain, and factor of safety across three design variants: one reference design and two modified alternatives developed based on technical criteria. The results are expected to inform design decisions, support prototype refinement, and contribute practical insights for improving the reliability of automation components in conveyor systems.

METHODS AND ANALYSIS

Materials

Mild steel was chosen as the main material for the stopper mounting component in this design because of its favorable blend of mechanical properties and ease of manufacturing. The choice of mild steel was also based on its wide market availability and excellent weldability. The mechanical properties of the mild steel are presented in Table 1 [20].

Table 1. Mechanical Properties Mild Steel

Properties	Mild steel	
	Units	Value
Mass Density	kg/m^3	7850
Young's Modulus	GPa	210
Poisson's Ratio		0,3
Tensile Yield Strength	MPa	250
Tensile Ultimate Strength	MPa	400
Weldment Strength	MPa	200
Weldment Design Strength	MPa	141

Modeling and Static Structural Analysis of Stopper Mounting

The stopper mounting design are modeled in Autodesk Inventor CAD software. Figure 1 shows the existing design (ED) of the stopper mounting that has been applied in an industrial conveyor system, with dimensions of 350 mm (length), 460 mm (width), and 620 mm (height).

Two modified variations were developed based on the initial design, each with a distinct geometric configuration, to compare their effectiveness and resistance under loading conditions. Versions 1 (MD 1) and versions 2 (MD 2) of the modified design are shown in Figure 2. Version 1 has the following dimensions: 381.2 mm length, 179.5 mm width, and 149.5 mm height. This design includes stiffening ribs that are strategically placed in areas susceptible to bending or fracture. Version 2 measures 381.2 mm in length, 106.5 mm in width, and 149.5 mm in height. It has a simpler structural approach that minimizes the use of additional reinforcing components. All three designs were exported in STEP format for further finite element analysis.

The design models were imported into ANSYS Static Structural, and the material properties were defined numerically using Table 1 data. The global coordinate system is defined as such: the X-axis represents the longitudinal direction of the stopper mounting frame, the Z-axis corresponds to the transverse direction, and the Y-axis denotes the vertical direction (height) aligned with the applied load. All deformation, strain, and stress evaluations were interpreted with respect to this coordinate reference system, as illustrated in Figure 1 and Figure 2. The loading applied to the stopper mounting structure was a force of 103.43 N, derived from the conversion of a total mass of 10.547 kg consisting of the pneumatic actuator, cover, and other supporting components. The placement of fixed support, applied loads, and meshing configurations were carried out as illustrated in Figure 3. The meshing process divides the model into smaller finite elements to achieve higher simulation accuracy. For the ED, the mesh utilized 211,334 nodes and 62,124 elements with a 4 mm element size. MD 1 used a finer mesh consisting

Figure 1. Existing stopper mounting design (ED)

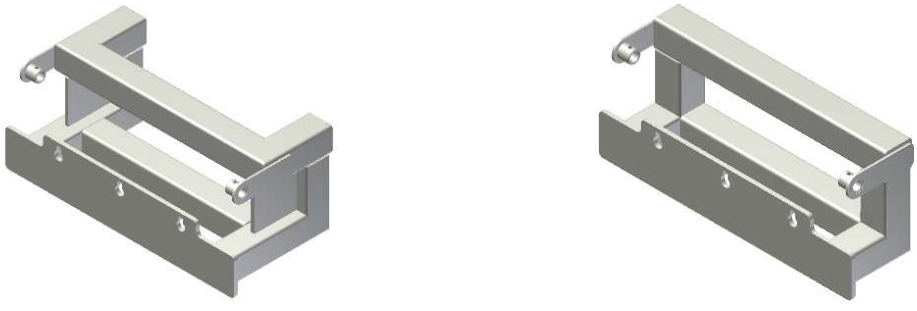

(a) (b)

Figure 2. (a) Stopper mounting design with stiffening ribs (MD 1); and (b) Stopper mounting design without stiffening ribs (MD 2)

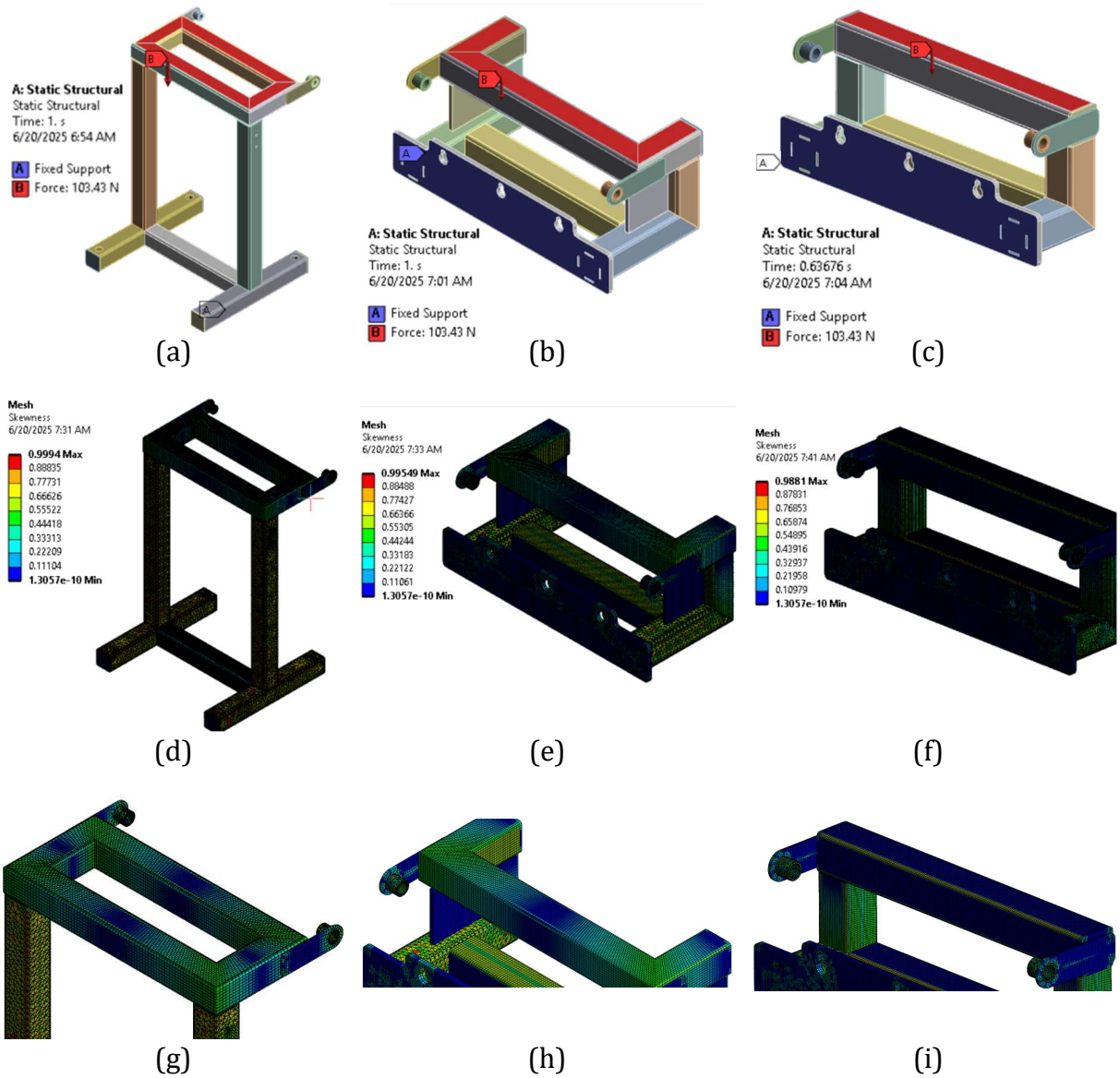

Figure 3. Load and boundary condition of (a) ED; (b) MD 1; (c) MD 2; mesh view model of (d) ED; (e) MD 1; (f) MD 2; and detail mesh view model of (g) ED; (h) MD 1; (i) MD 2

of 226,688 nodes and 46,521 elements at a resolution of 3 mm, and MD 2 used an even finer mesh with 414,014 nodes and 82,337 elements at a resolution of 2 mm. The mesh refinement was adjusted according to the overall dimensions of each design: larger structures were assigned coarser elements, while more compact geometries used finer meshes to capture structural behavior more precisely.

To evaluate the mechanical performance of each design variant, the static structural simulations in ANSYS generated four primary output parameters: total deformation, equivalent (von Mises) stress, elastic strain, and safety factor. These parameters were interpreted with reference to fundamental mechanical equations to validate the trends observed in the simulation. Total deformation under axial loading in linearly elastic components can be approximated by the classical mechanics formula:

$$\delta = \frac{F \cdot L}{A \cdot E} \tag{1}$$

where δ is the deformation (mm), F is the applied force (N), L is the original length of the component (mm), A is the cross-sectional area (mm^2), and E is the elastic modulus (MPa) [21]. Elastic strain was computed using the basic relation:

$$\varepsilon = \frac{\sigma}{E} \quad (2)$$

or

$$\varepsilon = \frac{l_1 - l_0}{l_0} \quad (3)$$

where ε is strain (dimensionless), Δl is the elongation (mm), and l_0 is the original length (mm) [21]. The equivalent stress observed in the model is conceptually derived from engineering stress, defined as:

$$\sigma = \frac{F}{A} \quad (4)$$

where σ is the stress (MPa), and A is the loaded area (mm^2) [21]. The safety factor (FoS) for each component was interpreted using the yield-based criterion:

$$\sigma_w = \frac{\sigma_y}{N} \quad (5)$$

$$N = \frac{\sigma_y}{\sigma_w} \quad (6)$$

where N is the factor of safety, σ_y is the material's yield strength (MPa), and σ_w is the equivalent stress obtained from the simulation (MPa) [21]. While the simulation captures more complex boundary conditions and multiaxial loading, these simplified equations serve as a theoretical basis to support the interpretation and validity of the FEA results.

RESULTS AND DISCUSSIONS

Evaluating Global Stiffness

The difference in deformation values between local maximum probes in a given design stems from the spatial distribution of structural response along the load path within the geometry. As shown in Table 2, the total deformation decreased by 88.42% and 88.61%, respectively, in MD 1 and MD 2 compared to ED. This significant reduction confirms the improvement in global stiffness performance across both modified geometries. Figure 4 clearly visualizes these trends with a comparative bar graph of defor-

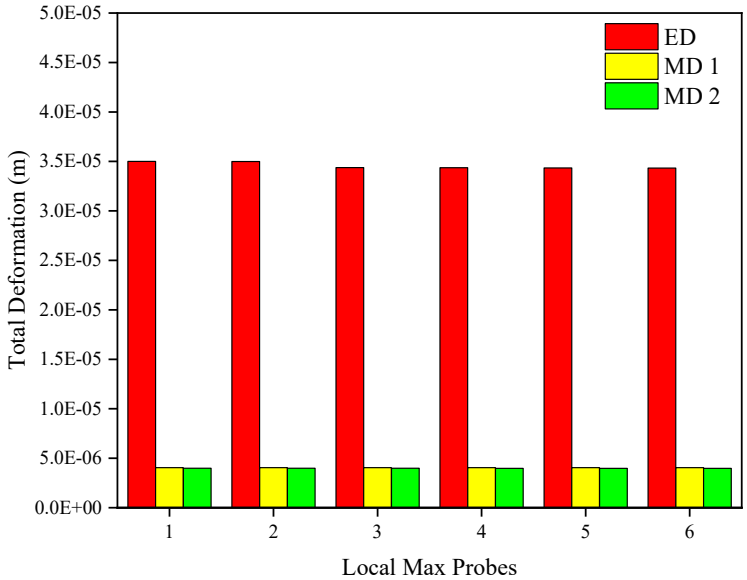

Figure 4. Comparison of total deformation values at six local max probes for each Stopper Mounting Design

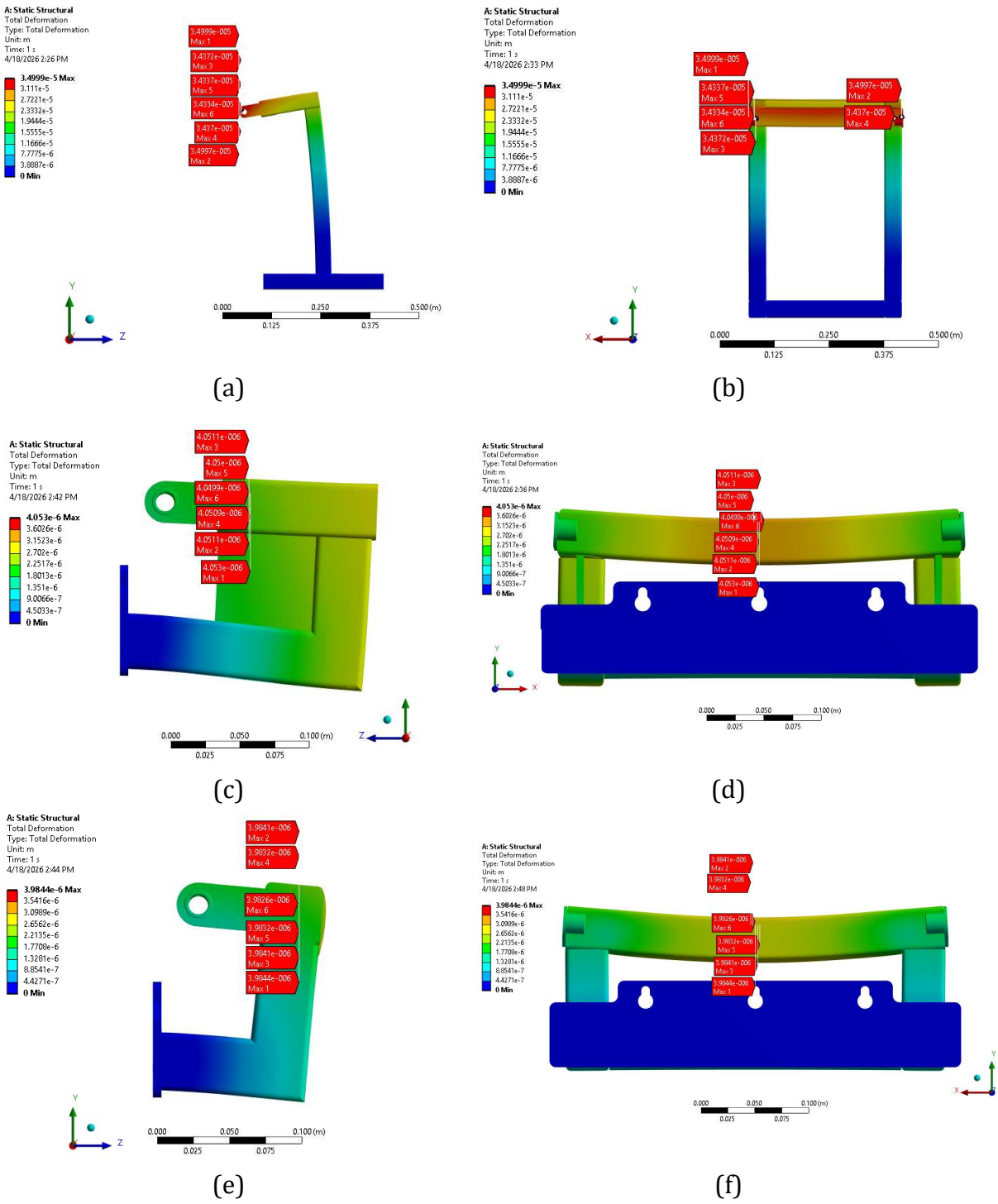

Figure 5. Side view deformation distribution for (a) ED; (c) MD 1; (e) MD 2; and front view deformation distribution for (b) ED; (d) MD 1; (f) MD 2

mation across all six local maximum probes, while Figure 5 supports these observations through contour plots illustrating the zones of highest deformation concentration in each configuration. In ED, the local maximum probes are predominantly located near the distal end of the stopper mounting. From a mechanical standpoint, this region behaves as a free-edge segment subjected to bending, where displacement accumulation is amplified due to limited structural restraint. Such deformation concentration at the terminal region is critical in practical applications, as excessive deflection at the stopper interface may affect alignment, contact stability, and long-term service reliability. In contrast, both MD 1 and MD 2 show probe concentration along the primary load path of the stopper mounting. This shift indicates that the incorporation of stiffening ribs increases sectional rigidity and

redistributes bending moments toward reinforced members, thereby stabilizing deformation patterns under static loading.

Table 2. Comparative matrix of structural performance parameters for stopper mounting designs

Parameter	Design	Local Max/Min Probes	Value
Maximum Total Deformation (m)	ED	1	3.49990E-05
		2	3.49970E-05
		3	3.43720E-05
		4	3.43700E-05
		5	3.43370E-05
		6	3.43340E-05
	MD 1	1	4.05300E-06
		2	4.05110E-06
		3	4.05110E-06
		4	4.05090E-06
		5	4.05000E-06
		6	4.04990E-06
	MD 2	1	3.98440E-06
		2	3.98410E-06
		3	3.98410E-06
		4	3.98320E-06
		5	3.98320E-06
		6	3.98260E-06
Maximum Equivalent Elastic Strain	ED	1	5.42120E-05
		2	4.22610E-05
		3	4.16230E-05
		4	3.72460E-05
		5	3.42210E-05
		6	2.42460E-05
	MD 1	1	2.54640E-05
		2	2.53720E-05
		3	2.51890E-05
		4	2.50770E-05
		5	2.36010E-05
		6	2.34230E-05
	MD 2	1	1.01880E-04
		2	1.01780E-04
		3	9.35610E-05
		4	9.34400E-05
		5	8.66780E-05
		6	8.66130E-05
Maximum Equivalent Stress (Pa)	ED	1	7.63680E+06
		2	7.63150E+06
		3	7.39540E+06
		4	7.15500E+06
		5	7.02170E+06
		6	6.77000E+06
	MD 1	1	5.28960E+06

Parameter	Design	Local Max/Min Probes	Value
		2	5.26620E+06
		3	4.95620E+06
		4	4.91890E+06
		5	4.81830E+06
		6	4.81460E+06
	MD 2	1	1.70620E+07
		2	1.70360E+07
		3	1.66170E+07
		4	1.65840E+07
		5	1.56520E+07
		6	1.56350E+07
Minimum Safety Factor	ED	1	0.88961
		2	0.9303
		3	0.96522
		4	0.97698
		5	0.99576
		6	1.0247
	MD 1	1	0.89801
		2	0.89856
		3	0.95186
		4	0.95259
		5	0.95495
		6	0.95705
	MD 2	1	0.90379
		2	0.90562
		3	0.95105
		4	0.95263
		5	0.9766
		6	0.97771

Small fluctuations in deformation values are attributed to variations in the X, Y, and Z coordinates, which alter the local bending moment distribution relative to the neutral axis. Because bending deflection is directly proportional to span length and inversely proportional to structural rigidity, even minor positional differences along the frame produce measurable variation in deformation magnitude. This aligns with Vieira et al. [22], who emphasized that slight positional changes can affect deformation modes and stiffness uniformity in structural systems. Meanwhile, although the modified forms have been strengthened, slight variations across probe points remain due to differences in stiffening rib orientation and support base geometry. The orientation of reinforcement modifies the local moment of inertia and load transfer efficiency, a behavior consistent with Nalepka et al. [23], who demonstrated that reinforcement orientation significantly influences local mechanical response. Local maximum probes that are clustered indicate a more controlled and directed load transfer mechanism, whereas dispersed probes reflect a broader and less constrained bending zone [24], [25]. The deformation contours in Figure 5 clearly show that deformation in ED extends toward the unreinforced edge, while in MD 1 and MD 2 it becomes confined within reinforced structural regions. Therefore, beyond merely reducing deformation magnitude, the modified designs improve structural robustness by relocating critical deformation away from vulnerable edge zones and into geometrically stabilized members. When designs are compared, the drastic decrease in deformation values from ED to the modified versions proves that

adding stiffening elements significantly enhances resistance to deformation. This simulation aligns with the findings of Lenkovskyi et al. [15], who reported that structural reinforcement reduces deformation in systems subjected to static loading, both locally and globally.

Mapping Local Flexibility

The variation in strain values among local maximum probes within each design originates from differences in internal force redistribution and localized bending response along the structural members [26]. It should be noted that identical material properties and boundary conditions were applied to ED, MD 1, and MD 2; therefore, differences in strain response arise solely from geometric modification and its influence on load transfer and sectional rigidity. Because strain represents the material-level response to structural deformation, its distribution is inherently linked to the deformation patterns discussed previously. Regions exhibiting higher curvature or concentrated displacement gradients tend to develop elevated tensile–compressive strain at their outer fibers. As shown in Table 2, the maximum strain decreased by 53.04% in MD 1 compared to ED, whereas MD 2 exhibited an 87.84% increase. These results indicate that geometric modification influences not only global stiffness but also the way deformation is transformed into localized material response. Figure 6 clearly visualizes the comparative strain magnitudes across all six local maximum probes, while Figure 7 supports these findings through contour plots illustrating spatial strain concentration in each configuration.

In ED, the local maximum strain probes are distributed across both the right and left vertical members, extending from the upper region toward the lower section. This pattern corresponds with the previously observed deformation behavior, where bending participation was spread along multiple vertical segments. From a mechanical standpoint, bending strain increases with curvature and with the distance of material fibers from the neutral axis. Because the vertical members in ED experience distributed lateral deflection, tensile and compressive strain gradients develop along both sides of the structure. The dispersed probe distribution therefore reflects a diffuse strain field, consistent with a broader and less constrained load transfer mechanism. This behavior aligns with Leutbecher and Schuller [27], who reported that slender and insufficiently braced members tend to develop widely distributed strain under bending loads.

In contrast, MD 1 exhibits significantly lower and more uniform strain values across

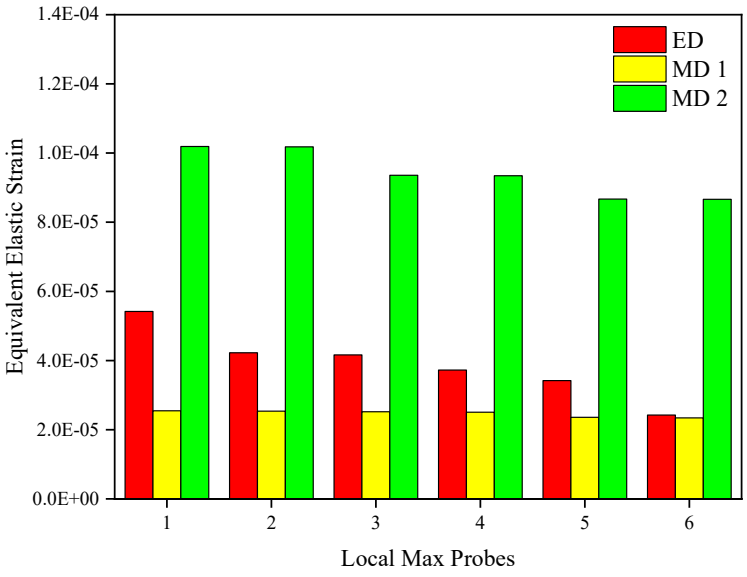

Figure 6. Comparison of equivalent elastic strain values at six local max probes for each stopper mounting design

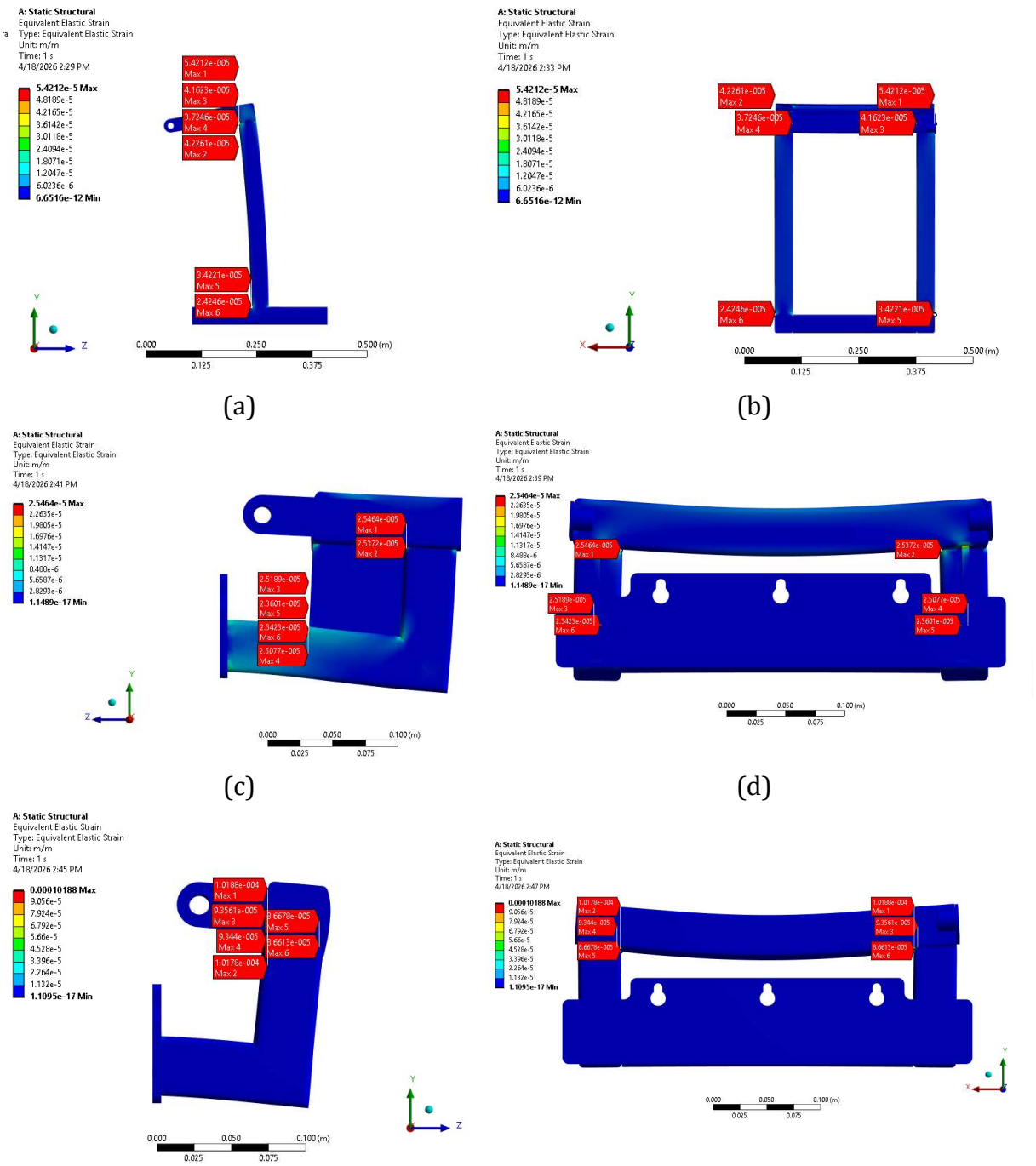

Figure 7. Side view elastic strain distribution for (a) ED; (c) MD 1; (e) MD 2; and front view elastic strain distribution for (b) ED; (d) MD 1; (f) MD 2

probe locations. As observed in the deformation analysis, the addition of stiffening ribs redirected bending moments toward reinforced members and increased sectional rigidity. The corresponding reduction in curvature leads to lower tensile–compressive strain gradients along the member thickness. In Figure 7, the local maximum strain probes become more centralized near the reinforced load path, particularly around the stiffening ribs, indicating a controlled and stabilized strain field. The closer spacing between probes suggests efficient load redistribution and improved structural balance. This observation is consistent with Legese et al. [28], who demonstrated that reinforcement elements enhance local stiffness and effectively suppress excessive strain concentration.

Meanwhile, MD 2 presents a contrasting mechanical response. Although global de-

formation is substantially reduced, strain values increase markedly at the monitored probes. As shown in Figure 7, the local maximum strain probes are strongly concentrated along the upper main span of the stopper mounting. This concentration corresponds with the deformation pattern previously identified, where displacement became confined along the primary load path. The simplified geometric configuration increases overall flexural rigidity and limits global deflection; however, it also restricts lateral load redistribution. As deformation becomes spatially confined, curvature is concentrated within a narrower structural region, intensifying localized fiber extension. Consequently, MD 2 behaves as a globally stiffer but strain-sensitive configuration. This stiffness–strain trade-off explains why reduced displacement does not necessarily result in reduced strain. Similar localization mechanisms due to geometric simplification were described by Samudin et al [29].

Small variations in strain magnitude are influenced by probe coordinates, which modify local bending orientation and internal force direction at each measurement point, as emphasized by Shi et al. [30]. Local maximum probes that are clustered indicate a directed and stabilized load transfer mechanism, whereas dispersed probes reflect broader strain participation across structural members [24], [25]. The strain contours in Figure 8 clearly demonstrate that ED exhibits a diffuse strain field along both vertical sides, MD 1 presents controlled strain near reinforced zones, and MD 2 shows concentrated strain along the upper span. Therefore, beyond merely comparing numerical strain values, analyzing strain distribution in relation to deformation patterns reveals how geometric modification reshapes internal force pathways. When the designs are compared, MD 1 achieves balanced and controllable local flexibility, whereas MD 2 enhances global stiffness at the expense of increased strain sensitivity in critical regions. This observation is consistent with Potirniche and Capatana's study [4], who emphasized that optimal structural performance requires equilibrium between global rigidity and local strain control.

Identifying Load Concentration Zones

The variation in equivalent stress values among local maximum probes reflects differences in internal force concentration along the structural load path. Because identical material properties and boundary conditions were applied to ED, MD 1, and MD 2, the observed stress variations originate purely from geometric modification and its influence on bending moment redistribution. In linear elastic behavior, stress is directly proportional to strain; therefore, the stress patterns observed here are mechanically consistent with the deformation and strain distributions discussed in the previous sections. As shown in Table 2, MD 1 reduces the maximum equivalent stress by 30.72% relative to ED, whereas MD 2 increases it by 123.39%. Figure 8 visualizes these differences through a comparative bar graph across the six local maximum probes, while Figure 9 illustrates the spatial stress concentration zones corresponding to those probe locations.

In ED, the difference between maximum stress probes exceeds 800,000 Pa, indicating uneven internal force participation across structural members. The stress probes are distributed along the vertical elements, reflecting a diffuse bending mechanism similar to the deformation and strain patterns previously identified. From a mechanical standpoint, bending stress increases proportionally with bending moment and distance from the neutral axis. Because ED allows distributed lateral deflection along relatively slender vertical members, bending moments are not effectively redirected toward specific reinforced regions. As a result, stress becomes moderately high but spatially dispersed. The spread of probe locations suggests uncontrolled force distribution across multiple members rather than a focused load path. This behavior is consistent with Lisyatnikov et al. [31], who demonstrated that variations in structural

stiffness directly influence local stress distribution in reinforced components.

In contrast, MD 1 exhibits lower and more stabilized equivalent stress values. As established in the deformation and strain analyses, the addition of stiffening ribs increases sectional rigidity and redirects bending moments toward reinforced zones. The improved moment of inertia reduces curvature and associated strain gradients, which consequently lowers stress magnitude. In Figure 9, the local maximum probes in MD 1 are clustered near the stiffeners, indicating that internal forces are effectively channeled into structurally stronger regions. The closer spacing between probes reflects a directed and controlled load transfer mechanism rather than diffuse force participation. This confirms that geometric reinforcement not only reduces global deformation but also mitigates local stress concentration. Such behavior aligns with the findings of Koulocheris and Vossou's study [20], who emphasized that internal reinforcement significantly improves force distribution and reduces localized high-stress risk.

Meanwhile, MD 2 presents a contrasting response. Although global deformation is reduced, the equivalent stress increases substantially, exceeding ED by 123.39%. As shown in Figure 9, stress probes are strongly concentrated along the upper main span of the structure. This concentration corresponds directly with the strain localization previously identified in the same region. The simplified geometry of MD 2 increases overall stiffness but reduces its ability to redistribute bending moments across multiple members. Consequently, internal forces become confined within a narrower structural segment. Because stress depends on both bending moment magnitude and sectional resistance, insufficient reinforcement combined with geometric transitions intensifies stress concentration. The close clustering of probes in this configuration indicates concentrated force channeling within a limited zone. Such localized high-stress regions are mechanically critical, as geometric discontinuities and abrupt stiffness changes can initiate failure, consistent with the findings of Shendy et al. [32], and Pardosi et al. [33].

Small variations in stress magnitude among probe points are influenced by positional differences in X, Y, and Z coordinates, which modify local bending orientation and internal force direction at each monitoring location. Probes that are clustered indicate focused load transfer and concentrated internal force pathways, whereas dispersed probes represent broader and less controlled stress participation across structural members. The contour plots in Figure 9 confirm this interpretation: ED exhibits distributed stress along vertical members, MD 1 presents moderated stress near reinfor-

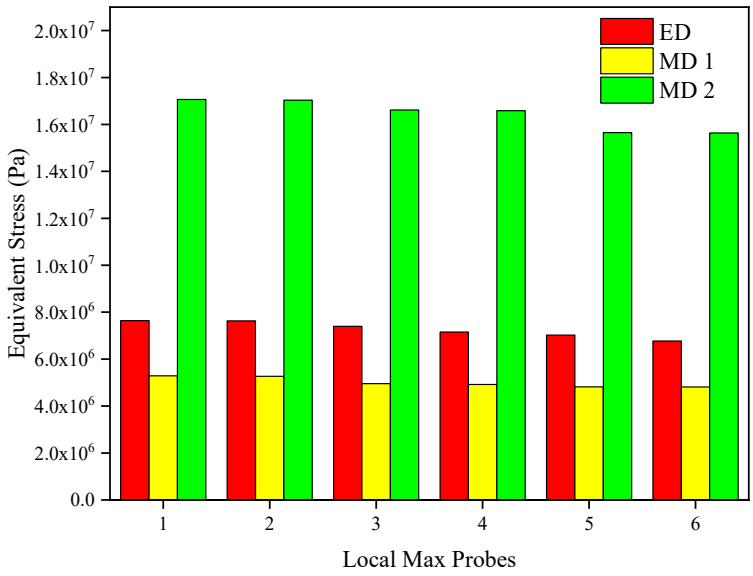

Figure 8. Comparison of equivalent stress values at six local max probes for each stopper mounting design

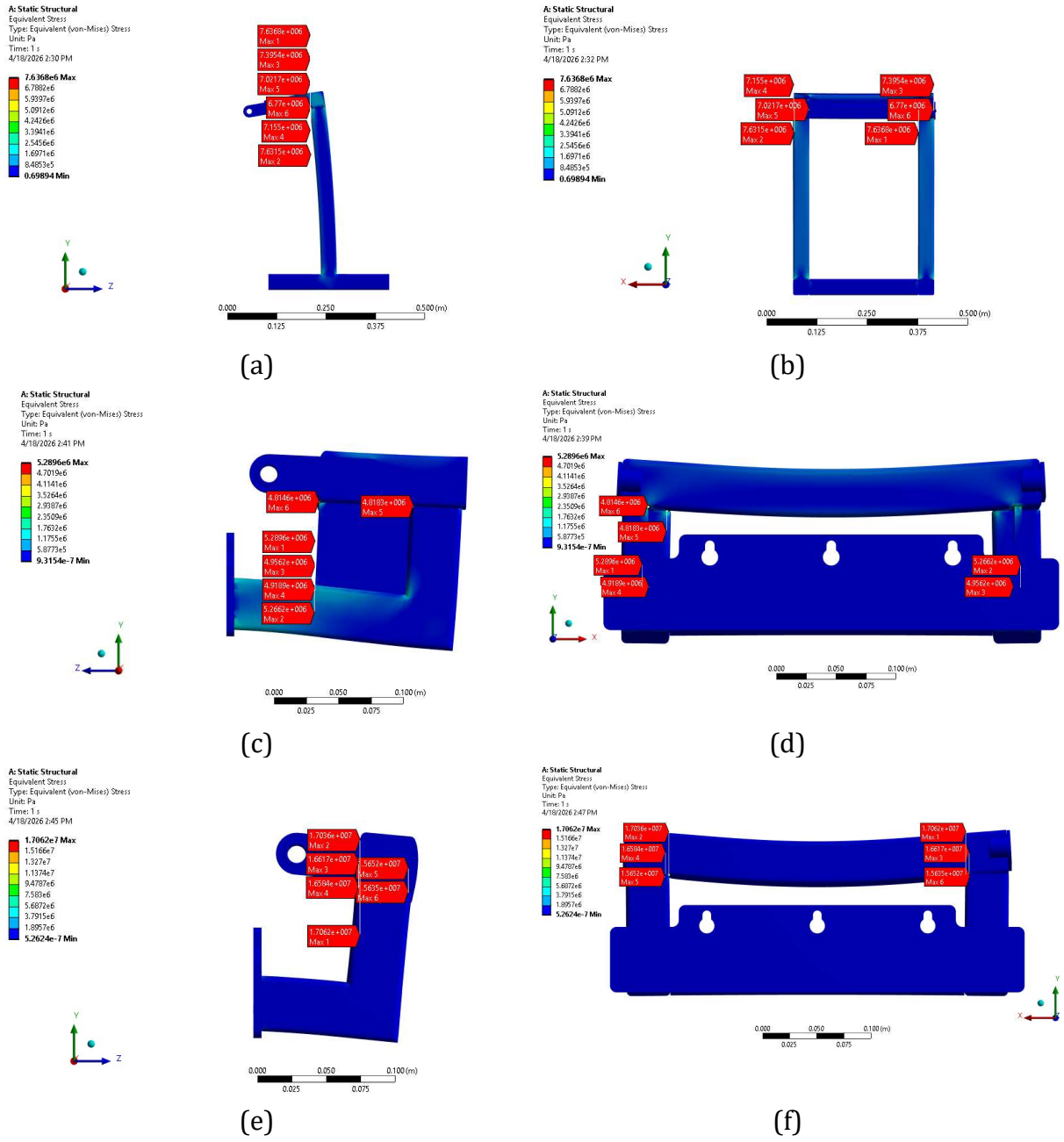

Figure 9. Side view stress distribution for (a) ED; (c) MD 1; (e) MD 2; and front view stress distribution for (b) ED; (d) MD 1; (f) MD 2

ced regions, and MD 2 shows pronounced stress concentration along the upper span. Therefore, integrating deformation, strain, and stress results reveals a coherent structural mechanism. ED demonstrates distributed flexibility with moderate but widespread stress participation. MD 1 achieves balanced structural performance by simultaneously reducing deformation, controlling strain, and stabilizing stress distribution through reinforcement. In contrast, MD 2 enhances global stiffness but at the expense of intensified load concentration in critical regions. This comparison highlights that effective structural optimization requires not only reducing displacement but also ensuring controlled internal force redistribution to prevent critical stress localization under static loading.

Assessing Structural Risk Margin

The structural risk margin is evaluated based on the simulated Safety Factor (FoS) distribution, where the minimum probe value is taken as the governing indicator of

structural reliability. Because identical material properties, yield strength, and boundary conditions were applied to ED, MD 1, and MD 2, differences in FoS arise solely from geometric modification and its effect on stress redistribution. In structural mechanics, failure initiates at the point where the ratio between material strength and equivalent stress is smallest; therefore, the minimum FoS determines the critical structural location. As shown in Table 2, the minimum FoS in MD 1 increased by 0.94% relative to ED, while MD 2 recorded a slightly higher increase of 1.59%. These variations are visualized in Figure 10 through the grouped column chart and spatially illustrated in the contour distribution of Figure 11.

In ED, the minimum safety factor falls slightly below unity, indicating that the maximum equivalent stress locally approaches or exceeds the allowable yield threshold. This behavior is mechanically consistent with the previously observed stress distribution, where internal forces were dispersed along the vertical members. Because stress governs FoS inversely, regions with higher stress concentration naturally correspond to lower safety margins [34]. The relatively scattered probe distribution in ED suggests that structural vulnerability is not confined to a single localized node but is distributed across multiple members, increasing the likelihood of critical stress participation under load.

In contrast, MD 1 exhibits a more stable and balanced FoS distribution, with values ranging from 0.89801 to 0.95705. As established in the stress analysis, the introduction of stiffening ribs improves bending moment redistribution and reduces stress magnitude. Since FoS is inversely proportional to equivalent stress, even moderate stress reduction directly increases the local safety margin. In Figure 11, the minimum FoS probes in MD 1 are more symmetrically positioned and relatively closer to one another, indicating a controlled and stabilized load transfer mechanism. The reduced variation between probe points reflects improved internal force equilibrium and suppression of localized overload. This mechanically consistent improvement aligns with reinforcement-based optimization studies such as those reported by Legese et al. [28], where geometric stiffening enhanced safety performance under static loading.

Meanwhile, MD 2 presents a more complex structural response. Although its minimum FoS slightly increases compared to ED, the dispersion between probe values remains relatively large. As shown in Figure 11, the critical safety factor region is concentrated along the upper primary span, corresponding to the previously identified stress concentration zone. The simplified geometry enhances global stiffness but restricts

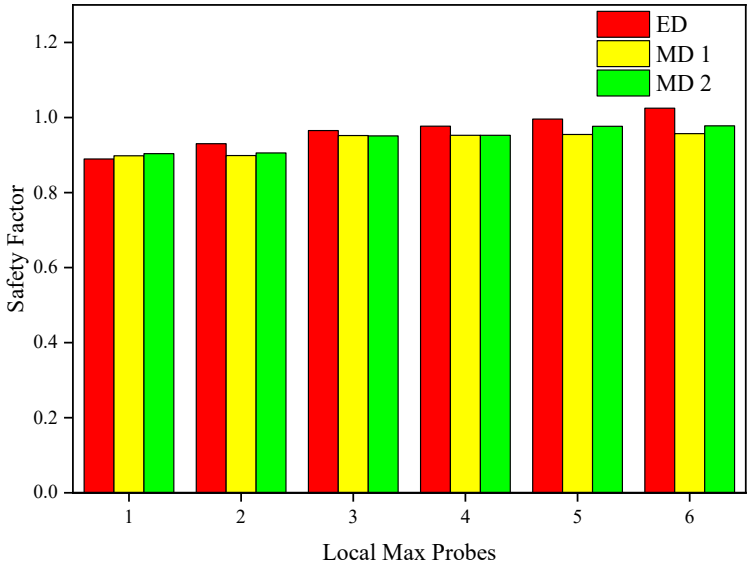

Figure 5. Comparison of safety factor at six local max probes for each stopper mounting design

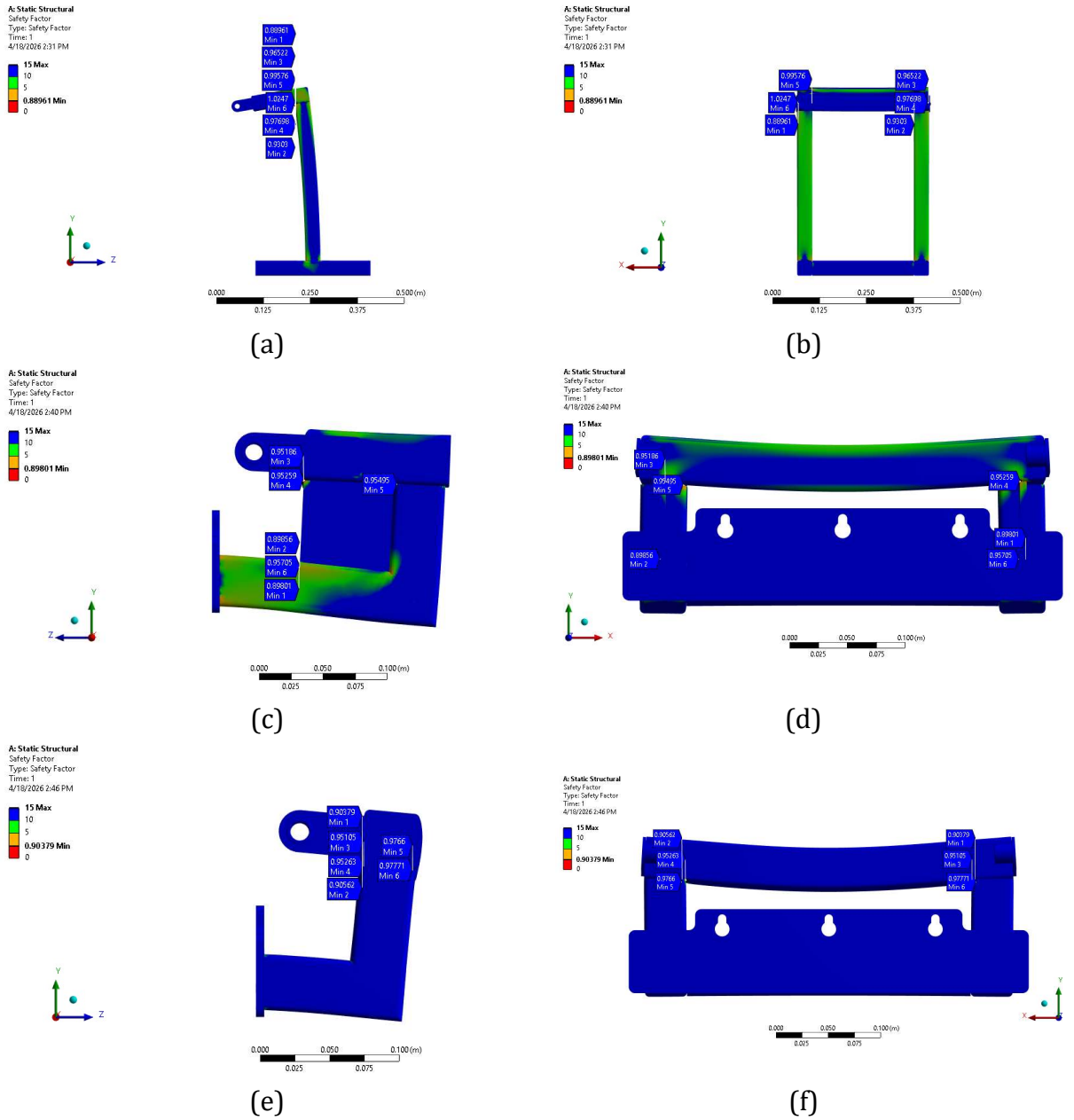

Figure 6. Side view safety factor distribution for (a) ED; (c) MD 1; (e) MD 2; and front view safety factor distribution for (b) ED; (d) MD 1; (f) MD 2

load redistribution, causing stress localization. Consequently, while some probe points show relatively high FoS values, the localized stress amplification reduces uniformity of the safety margin. This indicates that stiffness improvement alone does not guarantee balanced structural safety. The presence of concentrated critical zones suggests that MD 2 remains sensitive to overload initiation at specific locations.

Small variations in FoS among probes are influenced by positional differences in local stress magnitude along the Y and Z directions, which alter bending orientation and principal stress direction. However, structural reliability is governed by the minimum value rather than the average or maximum. As emphasized in stress-based safety assessments such as Matvienko [35], localized critical points determine the overall structural risk. The contour visualization in Figure 11 confirms the correlation between lower FoS values and previously identified stress concentration regions. Therefore, integrating deformation, strain, stress, and safety factor analyses reveals a consistent structural hierarchy. ED demonstrates distributed vulnerability with a minimum FoS below unity. MD 1 achieves a more balanced structural response by reducing stress

concentration and stabilizing the safety margin across probe locations. MD 2, although slightly improving the minimum FoS relative to ED, exhibits greater safety dispersion due to stress localization along the primary span. Among the evaluated configurations, MD 1 provides the most stable and controlled structural risk profile, indicating that reinforcement-based geometric optimization is more effective than geometric simplification in enhancing structural reliability under static loading conditions.

Design Comparison and Performance Synthesis

The comparative analysis of ED, MD 1, and MD 2 demonstrates how geometric modification governs structural behavior through the interconnected mechanisms of deformation, strain, stress, and safety factor. In ED, large total deformation occurs at the distal free-edge segment, where bending is unconstrained, leading to dispersed strain along vertical members and moderate but spatially spread stress, which collectively produce a minimum safety factor slightly below unity, indicating distributed vulnerability [36]. In MD 1, the introduction of stiffening ribs effectively confines deformation along reinforced load paths, reducing displacement magnitude and curvature, which in turn lowers tensile–compressive strain gradients and channels internal forces into structurally stronger regions, resulting in more uniform and moderated stress distribution and a stabilized safety factor across all probe locations [37], [38]. MD 2, while achieving the greatest reduction in global deformation, exhibits strain and stress localization along the upper main span, as the simplified geometry limits lateral load redistribution, generating high fiber extension and concentrated internal forces; consequently, the minimum safety factor shows greater dispersion despite increased global stiffness [39]. By reasoning through these coupled responses, it is evident that MD 1 achieves the optimal balance between global rigidity and local flexibility, minimizing deformation and strain while controlling stress concentrations and ensuring a uniform safety margin. From a practical perspective, this indicates that MD 1 provides a robust and reliable solution for conveyor mounting stoppers, maintaining precise alignment, reducing the risk of operational misalignment or premature wear, and ensuring consistent performance under dynamic loading conditions [36]. In contrast, ED remains susceptible to displacement and instability, while MD 2, despite high global stiffness, may develop critical stress concentrations that could compromise long-term service life [39].

CONCLUSIONS

This study systematically evaluated the structural performance of modified stopper mounting designs through finite element analysis, with particular emphasis on deformation, stress, and strain behavior under static loading conditions. The results provide clear insights into the effectiveness of different geometric modification strategies in enhancing structural integrity.

a. Test results indicate that the stiffening-rib configuration (MD 1) provides the most balanced structural performance, characterized by an 88.42% reduction in total deformation, a 53.04% decrease in equivalent elastic strain, and a 30.72% reduction in equivalent stress compared to the existing design (ED). These improvements confirm that reinforcement-based geometric modification effectively enhances global stiffness while simultaneously controlling local stress and strain behavior under static loading conditions.
b. The incorporation of stiffening ribs promotes more controlled internal force redistribution, confining deformation within reinforced load paths and preventing excessive strain–stress localization. In contrast, although MD 2 achieved a comparable 88.61% deformation reduction, it produced an 87.84% increase in strain and a 123.39% rise in equivalent stress, indicating that geometric simplification without adequate reinforcement intensifies load concentration along the primary span.

c. These findings confirm that structural optimization of stopper mounting components must balance global rigidity and local stress control. Reinforcement-oriented geometric design has proven more effective than geometric simplification in stabilizing deformation patterns, improving safety factor distribution, and enhancing structural reliability. The results provide a practical engineering basis for the development of precision-oriented conveyor subcomponents with improved durability and alignment stability in automated industrial systems.

ACKNOWLEDGEMENTS

DECLARATION OF CONFLICTING INTERESTS

The authors declare that they have no potential conflicts of interest regarding the research, authorship, and/or publication of this article.

FUNDING

REFERENCES

[1] A. N. Ciucu-Durnoi, C. Delcea, A. Stănescu, et al., "Beyond Industry 4.0: Tracing the Path to Industry 5.0 through Bibliometric Analysis," *Sustainability (Switzerland)*, vol. 16, no. 12, 2024, doi: 10.3390/su16125251.

[2] W. Kraus and T. Bauernhansl, "How Automation Will Change the Future of Production; [Wie Automatisierung die Zukunft der Produktion verändern wird Einordnung und Nutzen für produzierende Unternehmen]," *ZWF Zeitschrift fuer Wirtschaftlichen Fabrikbetrieb*, vol. 116, no. 10, pp. 652 – 656, 2021, doi: 10.1515/zwf-2021-0165.

[3] K. Chirumalla, H. Ali Jalil, and M. Behnam, "Navigating Production Automation as a Service: Unveiling Drivers, Benefits, and Challenges in Manufacturing Companies," in *Advances in Transdisciplinary Engineering*, J. Andersson, S. Joshi, L. Malmskold, and F. Hanning, Eds., IOS Press BV, 2024, pp. 206–218. doi: 10.3233/ATDE240166.

[4] M. A. Potirniche and G. F. Capatana, "STUDY OF THE BEHAVIOUR FOR THE WORK EQUIPMENT OF A FORKLIFT DURING THE WORKING PROCESS USING FINITE ELEMENT ANALYSIS," *International Journal of Modern Manufacturing Technologies*, vol. 14, no. 3, pp. 219–226, 2022, doi: 10.54684/ijmmt.2022.14.3.219.

[5] A. L. Zolkin, T. G. Aygumov, A. I. Adzhieva, et al., "Analysis of the integration of robotic automation in production," in *AIP Conference Proceedings*, I. Kovalev and A. Voroshilova, Eds., American Institute of Physics, 2024. doi: 10.1063/5.0199949.

[6] M. Sedore, "Automation in optical manufacturing: beveling and part handling," in *Proceedings of SPIE - The International Society for Optical Engineering*, J. D. G. Nelson and B. Unger, Eds., SPIE, 2023. doi: 10.1117/12.2684720.

[7] M. Sedore, "Applications of automation in optical manufacturing process chain: Grinding, polishing, and metrology," in *Proceedings of SPIE - The International Society for Optical Engineering*, J. D. Nelson and B. L. Unger, Eds., SPIE, 2021. doi: 10.1117/12.2602846.

[8] A. T. Ramadan, O. A. Alamri, and A. H. Tolba, "Reliability Assessment of Bridge Structure Using Bilal Distribution," *Mathematics*, vol. 12, no. 10, 2024, doi: 10.3390/math12101587.

[9] Z. Dogruyol and S. Güner, "Examining the impact of product variety on design, supply, and production processes using system dynamics approach," *Journal of the Faculty of Engineering and Architecture of Gazi University*, vol. 36, no. 3, pp. 1185–1198, 2021, doi: 10.17341/gazimmfd.731788.

[10] A. E. Baladeh and S. Taghipour, "Dynamic multilevel redundancy allocation optimization under uncertainty," in *Proceedings - Annual Reliability and Maintainability Symposium*, Institute of Electrical and Electronics Engineers Inc., 2023. doi: 10.1109/RAMS51473.2023.10088213.

[11] Nuroji, "Analysis of Reinforced Concrete Capacity for Irregular Cross-Sections Using Numerical Methods," in *Lecture Notes in Civil Engineering*, S. A. Kristiawan, B. S. Gan, M. Shahin, and A. Sharma, Eds., Springer Science and Business Media Deutschland GmbH, 2023, pp. 57–68. doi: 10.1007/978-981-16-9348-9_6.

[12] D. Zheng, "Design of Static Strength Analysis Software for Conveyor Head Tripod Based on ANSYS and MATLAB," in *Advances in Transdisciplinary Engineering*, C. C.-H., A. Scapellato, A. Barbiero, and D. G. Korzun, Eds., IOS Press BV, 2023, pp. 494–500. doi: 10.3233/ATDE230988.

[13] G. Fruet and L. Fleck Fadel Miguel, "Proposal of a methodology for mass optimization of realistic steel structural systems composed of columns and galleries for support of solid bulk conveyors," *Structures*, vol. 53, pp. 833–847, 2023, doi: 10.1016/j.istruc.2023.04.119.

[14] C. A. Wheeler , P. W. Robinson, P. J. Munzenberger et al., "Belt Conveyor Design and Troubleshooting," in *Simulations in Bulk Solids Handling: Applications of DEM and other Methods*, wiley, 2023, pp. 79–105. doi: 10.1002/9783527835935.ch3.

[15] T. M. Lenkovskyi, Y. L. Ivanytskyi, Y. V. Molkov et al., "Analysis of the Stress-Strain State of a Bridgman Specimen in Axial Tension by the Finite-Element Method," *Materials Science*, vol. 56, no. 5, pp. 722–726, 2021, doi: 10.1007/s11003-021-00488-4.

[16] P. Duranton, M. Bernion, A. Amzil, et al., "STRESS CLASSIFICATION PLANE CALCULATION AND VALIDATION," in *International Conference on Nuclear Engineering, Proceedings, ICONE*, American Society of Mechanical Engineers (ASME), 2023. [Online]. Available: https://www.scopus.com/inward/record.uri?eid=2-s2.0-85178518540&partnerID=40&md5=b199f9927db212185b765bd3728692f0

[17] M. Zubair, K. Singh, and A. K. Sehgal, "The Significance of Virtual Prototyping in reducing design risk and Accelerating Product Innovation," in *2023 14th International Conference on Computing Communication and Networking Technologies, ICCCNT 2023*, Institute of Electrical and Electronics Engineers Inc., 2023. doi: 10.1109/ICCCNT56998.2023.10306407.

[18] S. Pandey, N. K. Thakur, P. Nath, et al., "Optimizing Wind Load Performance through Shape Modifications and Corner Configurations in High-Rise Buildings: A Computational Fluid Dynamics Study," *Journal of The Institution of Engineers (India): Series A*, vol. 106, no. 2, pp. 631–648, 2025, doi: 10.1007/s40030-025-00884-y.

[19] Y. Li, X. Zhao, S. Liu, et al., "Review and Prospects of Numerical Simulation Research on Internal Flow and Performance Optimization of Twin-Screw Compressors," *Energies (Basel).*, vol. 18, no. 10, 2025, doi: 10.3390/en18102608.

[20] D. Koulocheris and C. Vossou, "Exploration of equivalent design approaches for tanks transporting flammable liquids," *Computation*, vol. 8, no. 2, Jun. 2020, doi: 10.3390/COMPUTATION8020033.

[21] W. D. Callister, *Materials Science and Engineering*, 10th ed. United States of America: Wiley, 2018.

[22] L. Vieira, R. Gonçalves, D. Camotim, et al., "Generalized Beam Theory deformation modes for steel–concrete composite bridge decks including shear connection flexibility," *Thin-Walled Structures*, vol. 169, 2021, doi: 10.1016/j.tws.2021.108408.

[23] K. Nalepka et al., "Ribs of Pinna nobilis shell induce unexpected microstructural changes that provide unique mechanical properties," *Materials Science and Engineering: A*, vol. 829, 2022, doi: 10.1016/j.msea.2021.142163.
[24] E. Putilova and K. Kryucheva, "Influence of Elastic–Plastic Deformation on the Structure and Magnetic Characteristics of 13Cr-V Alloyed Steel Pipe," *Symmetry (Basel).*, vol. 14, no. 6, 2022, doi: 10.3390/sym14061201.
[25] E. J. Sippel and H. B. Blum, "Structural analysis of steel structures with non-symmetric members," *Eng. Struct.*, vol. 245, 2021, doi: 10.1016/j.engstruct.2021.112739.
[26] N. A. Makhutov, "Analyzing Stress and Strain Concentration in the Inelastic Region for Strengthening and Softening Materials," *Journal of Machinery Manufacture and Reliability*, vol. 53, no. 2, pp. 107–113, 2024, doi: 10.1134/S1052618824020109.
[27] T. Leutbecher and J. Schuller, "Axial and f lexural tensile strength of thin members made of ultra-high-performance concrete; [Zug- und Biegezugfestigkeit dunner Tragelemente aus ultrahochfestem Beton]," *Betonwerk und Fertigteil-Technik/Concrete Plant and Precast Technology*, vol. 91, no. 3, p. 88, 2025, [Online]. Available: https://www.scopus.com/inward/record.uri?eid=2-s2.0-105004462113&partnerID=40&md5=e20bcd6e8f86721030620a526b7dd002
[28] A. M. Legese, A. Różański, M. Sobótka, et al., "Numerical analysis of soil–steel composite structure performance at ultimate load: impact of stiffening ribs and geotextile reinforcement," *Archives of Civil and Mechanical Engineering*, vol. 24, no. 3, 2024, doi: 10.1007/s43452-024-00986-7.
[29] I. Mat Samudin, N. A. Mohd Radzuan, A. B. Sulong, et al., "Stress strain curve analysis of sheet based TPMS structures in quasi static compression test: A review," *Journal of Materials Research and Technology*, vol. 36, pp. 5757–5796, May 2025, doi: 10.1016/j.jmrt.2025.04.168.
[30] Z. Shi, X. Xie, H. Zeng, et al., "Disaster mechanism of large-diameter shield tunnel segments under multi-source load coupling: A case study," *Eng. Fail. Anal.*, vol. 166, 2024, doi: 10.1016/j.engfailanal.2024.108878.
[31] M. Lisyatnikov, S. Roshchina, V. Martynov, et al., "Determination of Local Stresses in Places Where the Stiffness of Reinforced Wooden Beams Changes," in *Lecture Notes in Civil Engineering*, N. Vatin, S. Roshchina, and D. Serdjuks, Eds., Springer Science and Business Media Deutschland GmbH, 2024, pp. 235–247. doi: 10.1007/978-3-031-30570-2_21.
[32] M. Shendy, M. Alkhader, and B. A. Abu-Nabah, "Stress Concentration Induced by Synnergisticaly Interacting Geometric Discontinuites," in *2022 Advances in Science and Engineering Technology International Conferences, ASET 2022*, Institute of Electrical and Electronics Engineers Inc., 2022. doi: 10.1109/ASET53988.2022.9735055.
[33] V. H. Pardosi, S. Nugroho, and G. D. Haryadi, "ANALISIS KEGAGALAN VALVE IN (KATUP MASUK) PADA MOTOR KAPASITAS 155 CC," 2024.
[34] M. Amjad, S. Badshah, S. Ahmad et al., "Finite element modeling of stress distribution and safety factors in a Ti-27Nb alloy hip implant under real-world physiological loading scenarios," *PLoS One*, vol. 19, no. 8 August, Aug. 2024, doi: 10.1371/journal.pone.0300270.
[35] Y. G. Matvienko, "A Simplified Probabilistic Approach to Estimating the Safety Factors of Crack Resistance," *Journal of Machinery Manufacture and Reliability*, vol. 50, no. 3, pp. 200–207, 2021, doi: 10.3103/S1052618821030092.
[36] D. Pontan, *MANAJEMEN PROYEK KONSTRUKSI*, 1st ed. Medan: PT Media Penerbit Indonesia, 2024.
[37] A. Arwani, *INDUSTRI 4.0 BAGAIMANA MEREVOLUSI BISNIS ANDA*, 1st ed. Medan: PT Media Penerbit Indonesia, 2024.

[38] C. Kant and G. A. Harmain, "Fatigue Life Prediction Under Interspersed Overload in Constant Amplitude Loading Spectrum via Crack Closure and Plastic Zone Interaction Models-A Comparative Study," in *Lecture Notes in Mechanical Engineering*, A. W. M, Ed., Springer Science and Business Media Deutschland GmbH, 2022, pp. 253–260. doi: 10.1007/978-981-16-8810-2_18.

[39] A. M. Legese, A. Różański, M. Sobótka, et al., "Numerical analysis of soil–steel composite structure performance at ultimate load: impact of stiffening ribs and geotextile reinforcement," *Archives of Civil and Mechanical Engineering*, vol. 24, no. 3, 2024, doi: 10.1007/s43452-024-00986-7.

[40] X. Han, B. Han, Y. He, et al., "An Investigation into the Impact of Time-Varying Non-Conservative Loads on the Seismic Stability of Concrete-Filled Steel-Tube Arch Bridges," *Buildings*, vol. 14, no. 9, 2024, doi: 10.3390/buildings14092739.

[41] S. M. Harle, "Analyzing the Response of Structural Members to Impact Loads Using Finite Element Analysis: A Review," *Current Materials Science*, vol. 18, no. 1, pp. 53–75, 2025, doi: 10.2174/0126661454263264230926054553.